

DYNAMIC LINEAR REGRESSION MODELS FOR FORECASTING TIME SERIES WITH SEMI-LONG MEMORY ERRORS

THOMAS GOODWIN^{†‡}, MATIAS QUIROZ[‡] AND ROBERT KOHN^{†§}

ABSTRACT. Dynamic linear regression models forecast the values of a time series based on a linear combination of a set of exogenous time series while incorporating a time series process for the error term. This error process is often assumed to follow a stationary autoregressive integrated moving average (ARIMA) model, or its seasonal variants, which is unable to capture a long-range dependence structure (long memory) of the error process. We propose a novel dynamic linear regression model that incorporates the long-range dependence feature of the errors and show that the proposed error process may: (i) have a significant impact on the posterior uncertainty of the estimated regression parameters and (ii) improve the model's forecasting ability. We develop a Markov chain Monte Carlo method to fit general dynamic linear regression models based on a frequency domain approach that enables fast, asymptotically exact Bayesian inference for large datasets. We demonstrate that our approximate algorithm is faster than the traditional time domain approaches, such as the Kalman filter and the multivariate Gaussian likelihood, while producing a highly accurate approximation to the posterior. The method is illustrated in simulated examples and two energy forecasting applications.

Keywords: Bayesian inference, Frequency domain methods, Energy forecasting.

1. INTRODUCTION

Forecasting time series data plays an important role in various fields, such as engineering, economics, and climate sciences. Forecasting a single output time series may be more accurate by using linear combinations of exogenous variables that explain some of its historical variation (Hyndman and Athanasopoulos, 2021). However, the linear combination of the exogenous time series often does not capture all the serial correlation present in the output time series, resulting in autocorrelated errors. Dynamic linear regression models (Pankratz, 2012) provide a framework that relates the output time series to a linear combination of the exogenous time series and models the resulting error term as a time series process to account for serially correlated errors.

[†]: School of Economics, University of New South Wales.

[‡]: School of Mathematical and Physical Sciences, University of Technology Sydney.

[§]: Data Analytics Center for Resources and Environments (DARE).

Dynamic linear regression (DLR) models are a particular case of the more general class of transfer function models (Box et al., 2015).

The standard dynamic linear regression model assumes that the error process follows an autoregressive integrated moving average process (ARIMA). This approach allows the error process to have an autoregressive component and a moving average component for its white noise error term. While this error process accommodates a wide range of stationary processes, it requires a large number of autoregressive components to accommodate error processes that show significant autocorrelation between distant time periods. To capture such autocorrelations of the error process parsimoniously, we employ the autoregressive tempered fractionally integrated moving average (ARTFIMA) (Meerschaert et al., 2014; Sabzikar et al., 2019). The ARTFIMA class nests the well-known autoregressive fractionally integrated moving average (ARFIMA) (Granger and Joyeux, 1980) model, which is useful for time series with so-called long memory.

The ARTFIMA model has the following three advantages compared to the ARFIMA model, where the latter two are particularly important for the frequency domain estimation approach for dynamic linear regression models proposed in this paper. First, the autocovariance function of the ARFIMA model decays slowly as a power law (Granger and Joyeux, 1980) which is not absolutely summable. Such a process is referred to as having long memory (McLeod and Hipel, 1978). In contrast, the ARTFIMA model is appealing since its autocovariance function exhibits long-range dependence for several lags, but eventually decays exponentially fast (i.e. much faster than power law) and is hence absolutely summable. Such a process is referred to as having semi-long memory and is easier to analyse (Sabzikar et al., 2019). Second, the spectral density, also known as the power, of the ARFIMA process diverges as the frequency approaches zero. In practice, however, a stylised fact of the empirical power spectrum (the estimate of the spectral density) is that it is bounded for low frequencies. This is illustrated in Meerschaert et al. (2014) and Sabzikar et al. (2019), who show that the ARTFIMA process (whose spectral density does not diverge as the frequency approaches zero) fits the power spectrum better than the ARFIMA process for low frequencies; see also Figure 9 showing this carries over to the DLR case. This stylised fact is important for our purpose as we develop an estimation method based on a parametric Whittle likelihood (Whittle, 1953), which is a frequency domain approximation of the time domain likelihood that represents the information in the data via the spectral density. Third, the Whittle approximation fails to hold for long memory processes, especially for small frequencies (Robinson, 1995; Rousseau et al., 2012). Section 4.2 demonstrates this drawback for DLR models based on ARFIMA errors via a simulation study and also shows that ARTFIMA errors overcomes this issue. We show that resorting to the time domain

likelihood for estimating a dynamic linear regression with ARFIMA errors (Doornik and Ooms, 2003) is computationally much more costly than our frequency domain approach. Moreover, in terms of prediction accuracy, our model is often superior, or at least on par with DLR with ARFIMA and ARMA errors.

The parameters in dynamic linear regression models consist of the regression coefficients that form the linear combination of the exogenous time series and the parameters of the error process. For the standard dynamic linear regression models with ARIMA errors that are normally distributed, efficient likelihood-based inference can be carried out by finding the finite-dimensional state space representation of the model and using the Kalman filter to integrate out the unobserved time-varying error terms (Anderson and Moore, 2005). This may still be computationally costly with many time observations, especially in Bayesian inference, which typically requires many posterior samples for reliable inference. For each such sample, the Kalman filter needs to cycle through all the observations, which can be prohibitively expensive, especially for large time series. The Whittle log-likelihood can be derived using large sample properties of the so-called periodogram data, which are formed via the discrete Fourier transform of the time domain data. The Whittle log-likelihood is directly a function of the regression coefficients and the error process parameters without needing to integrate out unobserved error terms. However, in DLR models, the periodogram data becomes a function of the regression coefficients, which requires recomputing the discrete Fourier transform in every iteration. We show how this can be avoided, and thus our algorithm requires computing the discrete Fourier transform only once before running the sampling algorithm, thereby obtaining significant computational gains compared to the time domain log-likelihood based on the Kalman filter. Our frequency domain approach also applies to a dynamic linear regression model with ARTFIMA errors, where a finite-dimensional state space representation is not readily available.

To summarise, our article makes two important contributions. First, we propose a frequency domain estimation approach for dynamic linear models that significantly outperforms estimation approaches based on the time domain likelihood in terms of computing time, especially when a finite-dimensional state space representation of the model is unavailable. Second, we utilise a semi-long memory process for the error process and show that it may provide more accurate forecasts compared to both the standard dynamic linear model and that of using a long memory process for the error term, especially for datasets with complex long-range dependence. Moreover, we demonstrate that the semi-long memory process may significantly impact the posterior distribution of the regression parameters.

The rest of the article is organised as follows. Section 2 reviews existing dynamic linear models and presents our extension. Section 3 introduces the necessary frequency domain tools, outlines our estimation method, and validates its performance relative to the time domain likelihood. Section 4 includes relevant simulation studies. Section 5 presents applications for two real-world electricity demand datasets.

2. DYNAMIC LINEAR REGRESSION MODELS

2.1. Standard dynamic linear regression models. Let $\mathbf{X}_t = (X_{1t}, \dots, X_{mt})^\top \in \mathbb{R}^m$ be a set of m exogenous stationary time series observed at time t . A dynamic linear regression models the scalar output time series $Y_t \in \mathbb{R}$ as a linear combination of the exogenous \mathbf{X}_t , i.e.

$$Y_t = \mathbf{X}_t^\top \boldsymbol{\beta} + \eta_t, \quad (2.1)$$

where $\boldsymbol{\beta} \in \mathbb{R}^m$ is a vector of regression coefficients and $\eta_t \in \mathbb{R}$ is a zero-mean error process. The error process contains all unobserved factors that affect Y_t , and we assume that $E(\eta_t | \mathbf{X}_t) = 0$, i.e. it is uncorrelated with each of the elements in \mathbf{X}_t and hence \mathbf{X}_t is exogenous.

When the error process η_t is an independent series, (2.1) is a standard linear regression (if it has a constant variance) and can easily be estimated using standard linear regression approaches (or modified versions thereof if heteroscedasticity is present). However, in many applications, the unobserved factors are time-varying, resulting in serially correlated errors η_t . The standard dynamic linear regression model assumes that η_t is an autoregressive integrated moving average process, denoted $\text{ARIMA}(p, d, q)$ and defined as

$$\phi_p(B) \Delta^d \eta_t = \psi_q(B) \varepsilon_t, \quad (2.2)$$

where $\phi_p(B) = 1 - \sum_{i=1}^p \phi_i B^i$ and $\psi_q(B) = 1 + \sum_{i=1}^q \psi_i B^i$ are the autoregressive and moving average lag polynomials, respectively, with the lag operator B such that $B^i \eta_t = \eta_{t-i}$. The differencing operator Δ^d , for $d = 0, 1, 2, \dots$, is defined as $\Delta^d \eta_t = (1 - B)^d \eta_t$. Finally, ε_t is the white noise error. When the error process η_t exhibits seasonality with seasonal period s , this can be modelled by a seasonal ARIMA process, denoted $\text{ARIMA}(p, d, q)(P, D, Q)_s$ and defined as

$$\phi_p(B) \phi_P^*(B^s) \Delta^d \Delta_s^D \eta_t = \psi_q(B) \psi_Q^*(B^s) \varepsilon_t, \quad (2.3)$$

where $\phi_P^*(B^s) = 1 - \sum_{i=1}^P \phi_i^* B^{is}$ and $\psi_Q^*(B^s) = 1 + \sum_{i=1}^Q \psi_i^* B^{is}$ are the seasonal autoregressive and seasonal moving average lag polynomials, and $\Delta_s^D = (1 - B^s)^D$, for $D = 0, 1, 2, \dots$, is the seasonal differencing operator (Box et al., 2015).

To carry out inference in (2.1), it is typically assumed that η_t is normally distributed. The resulting log-likelihood is then a multivariate Gaussian distribution with a Toeplitz covariance matrix given that η_t , or after integer differencing of η_t , is stationary (Doornik and Ooms, 2003). Inversion of such a matrix is usually performed via the Levinson-Durbin algorithm (Levinson, 1946; Durbin, 1960) in $\mathcal{O}(T^2)$ operations. However, recent approaches, known as superfast Toeplitz algorithms, can solve the matrix system in $\mathcal{O}(T \log_2^2(T))$ operations, which becomes more efficient than the Levinson-Durbin algorithm when $T > 256$ (Ammar and Gragg, 1988). A method that scales even better is to find the finite-dimensional state space representation of the model in (2.1) with the error process following either (2.2) or (2.3), in which the resulting likelihood can be evaluated in $\mathcal{O}(T)$ using the Kalman filter.

2.2. Long memory dynamic linear regression models. In many applications, a pair of observations separated by a long time interval exhibit a non-negligible correlation. The standard dynamic linear regression model with the error process in (2.2) has an autocovariance function whose absolute value decays exponentially fast and thus cannot capture this feature. A common approach to model time series with long memory is to consider so-called fractional differencing.

In a dynamic linear regression setting, Doornik and Ooms (2004) propose to model the error process η_t in (2.1) with an autoregressive fractionally integrated moving average process (Granger and Joyeux, 1980; Hosking, 1981), denoted ARFIMA(p, d, q). This model is, for $d \notin \mathbb{Z}$,

$$\phi_p(B)\Delta^d\eta_t = \psi_q(B)\varepsilon_t, \quad (2.4)$$

where $\phi_p(B)$ and $\psi_q(B)$ are defined as in (2.2). The fractional differencing operator is defined via the fractional binomial theorem

$$\begin{aligned} \Delta^d\eta_t &= (1 - B)^d\eta_t \\ &= \sum_{j=0}^{\infty} \binom{d}{j} (-B)^j \eta_t \\ &= \sum_{j=0}^{\infty} (-1)^j \frac{\Gamma(1+d)}{\Gamma(1+d-j)j!} \eta_{t-j}, \end{aligned}$$

where $\Gamma(a) = \int \exp(-t)t^{a-1}dt$ using $a! = \Gamma(1+a)$. Provided that the roots of $\phi_p(z)$ are outside the unit circle, the ARFIMA process is stationary if $-0.5 < d < 0.5$ and has long memory when $0 < d < 0.5$ (Granger and Joyeux, 1980). Doornik and Ooms (2004) also propose a seasonal extension by modelling η_t as a seasonal ARFIMA(p, d, q)(P, D, Q)_s with $d \notin \mathbb{Z}$ and integer D . A possible extension of this model is to allow for non-integer D as in Bisognin and Lopes (2009).

Doornik and Ooms (2003) show that maximum likelihood estimation for ARFIMA models is possible in $\mathcal{O}(T^2)$ time, and this also applies for the model in (2.1) with the error process following (2.4). Chan and Palma (1998) show that there is no finite-dimensional state space representation of an ARFIMA process. They propose an infinite-dimensional state space representation for which the Kalman filter can be computed in T steps; however, the resulting computation is $\mathcal{O}(T^3)$.

2.3. Semi-long memory dynamic linear regression models. The autoregressive tempered fractional integrated moving-average (Meerschaert et al., 2014; Sabzikar et al., 2019) (ARTFIMA) extends the ARFIMA model, incorporating a tempering parameter λ . The model for the error process is then

$$\phi_p(B)\Delta^{d,\lambda}\eta_t = \psi_q(B)\varepsilon_t, \quad (2.5)$$

where $\phi_p(B)$ and $\psi_q(B)$ are defined as in (2.2) and for $d \notin \mathbb{Z}$ and $\lambda > 0$ the tempered fractional differencing operator is

$$\begin{aligned} \Delta^{d,\lambda}\eta_t &= (1 - \exp(-\lambda)B)^d \eta_t \\ &= \sum_{j=0}^{\infty} \binom{d}{j} (-B)^j \eta_t \\ &= \sum_{j=0}^{\infty} (-1)^j \frac{\Gamma(1+d)}{\Gamma(1+d-j)j!} \exp(-\lambda j) \eta_{t-j}. \end{aligned} \quad (2.6)$$

Note that when $\lambda = 0$, the ARTFIMA model is a stationary ARFIMA model if $-0.5 < d < 0.5$, provided the roots of the polynomial $\phi_p(z)$ are outside the unit circle. When $\lambda = 0$ and d is an integer, the ARTFIMA model becomes an ARIMA model. The ARTFIMA model is stationary for all $d \notin \mathbb{Z}$ and $\lambda > 0$ provided that the root condition of the polynomial $\phi_p(z)$ is satisfied (Sabzikar et al., 2019). Section 1 outlines the advantages the ARTFIMA process has over ARFIMA.

Similarly to the ARFIMA model, a finite-dimensional state space representation that allows efficient Kalman filter computations is unavailable for the ARTFIMA model. Instead, the log-likelihood can be computed using a multivariate Gaussian distribution with a Toeplitz covariance matrix formed via the autocovariance function in Sabzikar et al. (2019, Theorem 2.5 (b)). However, Section 3 describes a more computationally efficient approach based on a frequency domain log-likelihood for the periodogram data. The approach relies on the spectral density of the process, which we now describe.

Let ω denote an angular frequency. The spectral density $f(\omega)$ is the Fourier transform of the covariance function and shows how the variance of the time series is distributed among the frequencies $-\pi \leq \omega \leq \pi$. The spectral density when η_t follows the

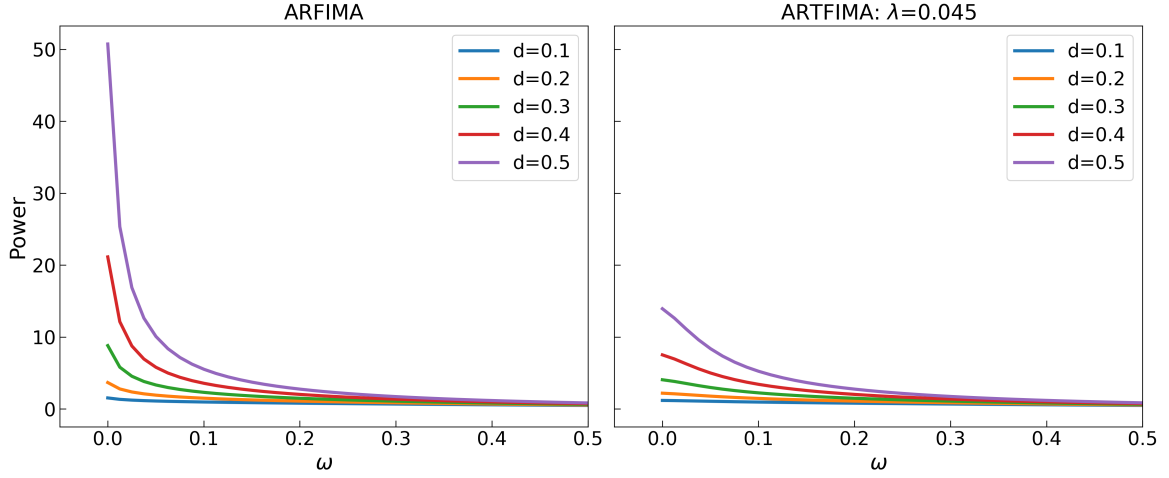


FIGURE 1. Spectral densities of ARFIMA and ARTFIMA models with $p = 1$ and $q = 0$. For both processes, $\phi = 0.5$ and ARTFIMA $\lambda = 0.045$.

ARTFIMA process in (2.5) is (Sabzikar et al., 2019, Theorem 2.5 (a))

$$f(\omega; \boldsymbol{\theta}) = \frac{\sigma_\varepsilon^2}{2\pi} \left| 1 - e^{-(\lambda + i\omega)} \right|^{-2d} \left| \frac{\psi_q(e^{-i\omega})}{\phi_p(e^{-i\omega})} \right|^2, \quad (2.7)$$

with parameter vector $\boldsymbol{\theta} = (\phi_1, \dots, \phi_p, \psi_1, \dots, \psi_q, d, \lambda, \sigma_\varepsilon^2)^\top$, where $\sigma_\varepsilon^2 = \text{Var}(\varepsilon_t)$ and $i^2 = -1$. The seasonal ARTFIMA(p, d, q)(P, D, Q) $_s$, with $d \notin \mathbb{Z}$ and integer D ,

$$\phi_p(B)\phi_p^*(B^s)\Delta^{d,\lambda}\Delta_s^D\eta_t = \psi_q(B)\psi_q^*(B^s)\varepsilon_t, \quad (2.8)$$

where all quantities have been previously defined. The spectral density of $\Delta_s^D\eta_t$ in (2.8) is

$$f(\omega; \boldsymbol{\theta}) = \frac{\sigma_\varepsilon^2}{2\pi} \left| 1 - e^{-(\lambda + i\omega)} \right|^{-2d} \left| \frac{\psi_q(e^{-i\omega})\psi_q^*(e^{-is\omega})}{\phi_p(e^{-i\omega})\phi_p^*(e^{-is\omega})} \right|^2. \quad (2.9)$$

Figure 1 shows the spectral density for both the ARFIMA and ARTFIMA process for different values of the fractional differencing parameter d . An important difference that we have stressed is the limiting behaviour as $\omega \rightarrow 0$, where the spectral density of the ARFIMA process diverges when $d > 0$, whereas that of the ARTFIMA process does not. When estimating the power for real data, it is often observed to be bounded as discussed in Section 1. Hence, the ARTFIMA model provides a better fit for small frequencies; see, for example, Figure 9.

3. METHODOLOGY

3.1. Frequency domain likelihood. The frequency domain approach to inference relies on the asymptotic properties of the frequency representation of the time series process in (2.1). Engle (1974) shows how to rewrite (2.1) in terms of the periodograms of Y_t and X_t and derive the ordinary least squares estimator of the transformed regression, which is also shown to be the best linear unbiased estimator. Our Bayesian approach requires a log-likelihood function, which can be derived using asymptotic properties of the periodogram data, and is outlined below.

Let Y_t and X_t be zero-mean processes. Suppose that β is known and define the pseudo data

$$Z_t = Y_t - X_t^\top \beta, \quad t = 1, \dots, T. \quad (3.1)$$

The non-seasonal ARTFIMA process has the spectral density in (2.7), and when $\lambda = 0$ and $d = 0$, it simplifies to the spectral density for a non-seasonal ARMA model. The general case assumes that η_t is a seasonal ARTFIMA process and has the spectral density given by (2.9). Similarly, the spectral density of the seasonal ARMA process is obtained by setting $\lambda = 0$ and $d = 0$.

Recall $\omega \in [-\pi, \pi]$ as the angular frequency and denote the natural Fourier frequencies as $\omega_k = \frac{2\pi k}{T}$ for $k \in \mathcal{K}$, where

$$\mathcal{K} = \begin{cases} -\frac{T}{2}, -\frac{T}{2} + 1, \dots, \frac{T}{2} - 1, & \text{if } T \text{ is even,} \\ -\frac{(T-1)}{2}, -\frac{(T-1)}{2} + 1, \dots, \frac{(T-1)}{2}, & \text{if } T \text{ is odd.} \end{cases} \quad (3.2)$$

The frequency representation of the time series process Z_t is obtained via its discrete Fourier transform (DFT), which is the complex-valued transform

$$J_Z(\omega_k) = \sum_{t=1}^T Z_t \exp(-i\omega_k t), \quad (3.3)$$

and can be computed for all T frequencies $\omega_k, k \in \mathcal{K}$, using $\mathcal{O}(T \log_2(T))$ operations via the fast Fourier transform (Cooley and Tukey, 1965). Since the pseudo data depends on β , the DFT in (3.3) needs to be recomputed for each new sample in the Markov chain Monte Carlo (MCMC) algorithm. However, following Matsuda and Yajima (2009),

$$\begin{aligned} J_Z(\omega_k) &= \sum_{t=1}^T (Y_t - X_t^\top \beta) \exp(-i\omega_k t) \\ &= \sum_{t=1}^T Y_t \exp(-i\omega_k t) - \left(\sum_{t=1}^T X_t \exp(-i\omega_k t) \right)^\top \beta \\ &= J_Y(\omega_k) - J_X(\omega_k)^\top \beta, \end{aligned}$$

where J_Y is the DFT of Y_t , and $J_X(\omega_k)$ is the m -dimensional column vector with the j th element being the DFT of the (univariate) time series X_{jt} . Thus, since $J_Y(\omega_k)$ and $J_X(\omega_k)$ only depend on the data Y_t and X_t , and can be pre-computed before the MCMC algorithm, $J_Z(\omega_k)$ can be evaluated in $\mathcal{O}(T)$ for all frequencies when β changes (assuming $m \ll T$).

Let $\Re(J_Z(\omega_k))$ and $\Im(J_Z(\omega_k))$ be the real and imaginary parts of the DFT $J_Z(\omega_k)$ which is a weighted complex valued sum of the pseudo data. Peligrad and Wu (2010, Theorem 2.1) show that under some regularity conditions,

$$\frac{1}{\sqrt{T}}(\Re(J_Z(\omega_k)), \Im(J_Z(\omega_k))), \quad T \rightarrow \infty, \quad (3.4)$$

converge in distribution to a bivariate normal distribution with (asymptotically) independent components having expected value 0 and variance $\pi f(\omega_k)$, with f being the spectral density of Z_t . Moreover, they show that the $\frac{1}{\sqrt{T}}J_Z(\omega_k)$ are asymptotically independent for all $k \in \mathcal{K}$.

Define the periodogram

$$I_Z(\omega_k) = \frac{1}{2\pi} \left| \frac{1}{\sqrt{T}} J_Z(\omega_k) \right|^2. \quad (3.5)$$

Then, for $k \in \mathcal{K} \setminus 0$, by (3.4),

$$\frac{I_Z(\omega_k)}{f(\omega_k)} = \frac{1}{2} \left| \frac{1}{\sqrt{\pi f(\omega_k)}} \frac{1}{\sqrt{T}} J_Z(\omega_k) \right|^2 \sim \frac{\chi^2(2)}{2}, \quad (3.6)$$

as $T \rightarrow \infty$, where $\chi^2(\nu)$ denotes the chi-squared distribution with ν degrees of freedom. Note that $\nu = 2$ follows from $|\cdot|^2$ in (3.6) being a sum of two squared (asymptotically) independent standard normal random variables when $k \in \mathcal{K} \setminus 0$. Since $\frac{\chi^2(2)}{2}$ is a standard exponential random variable, it follows that

$$I_Z(\omega_k) \sim \text{Exp}(f(\omega_k)), \quad k \in \mathcal{K} \setminus 0, \quad (3.7)$$

where $\text{Exp}(f(\omega_k))$ denotes an exponential distribution with mean $f(\omega_k)$. Emphasising the dependence on the parameters, the log-density of (3.7) is

$$\log p(I_Z(\omega_k; \beta) | \theta) = -\log(f(\omega_k; \theta)) - \frac{I_Z(\omega_k; \beta)}{f(\omega_k; \theta)}, \quad k \in \mathcal{K} \setminus 0, \quad (3.8)$$

where $\theta = (\boldsymbol{\vartheta}^\top, \boldsymbol{\beta}^\top)^\top$ contains all unknown parameters. When $k = 0$, $J_Z(0) = 0$ since $J_Y(0) = \sum_{t=1}^T Y_t = 0$ and $J_X(0) = \sum_{t=1}^T \mathbf{X}_t = \mathbf{0}$ for demeaned data.

The asymptotic distributions of the periodogram data underlie the idea of the so-called Whittle log-likelihood (Whittle, 1953): use the log-density of each periodogram observation $I_Z(\omega_k; \beta)$ in (3.8) to form the log-likelihood of all periodograms, which

becomes a sum due to the (asymptotic) independence. For a real-valued process Z_t , both the periodogram and spectral density are symmetric around the origin; hence, only non-negative frequencies are considered. The Whittle log-likelihood is obtained by adding (due to the asymptotic independence) the log-densities in (3.8) for all the positive frequencies (zeroth frequency excluded with demeaned data). The Whittle log-likelihood is, for odd T ,

$$\ell_W(\boldsymbol{\theta}) = - \sum_{k=1}^{(T-1)/2} \left(\log(f(\omega_k; \boldsymbol{\theta})) + \frac{I_Z(\omega_k; \boldsymbol{\beta})}{f(\omega_k; \boldsymbol{\theta})} \right), \quad (3.9)$$

and the summation runs to $T/2 - 1$ instead if T is even. Guyon (1982) and Kent and Mardia (1996) show that the Whittle log-likelihood is a spectral approximation of the Gaussian time domain log-likelihood. In particular, they derive probabilistic convergence results of, respectively, the Whittle log-likelihood and its derivative, to the Gaussian log-likelihood and its derivative.

Finally, we stress that a frequency domain approach via the Whittle log-likelihood for dynamic linear regression models is inappropriate when using the ARFIMA model, because the Whittle approximation fails to hold for long memory processes, in particular for the small frequencies (Robinson, 1995; Rousseau et al., 2012). Thus, to carry out inference in dynamic linear regression models with ARFIMA errors, it is necessary to use the time domain log-likelihood, which is considerably slower to compute compared to a frequency domain approach that uses the ARTFIMA process; see Sections 4.1, 5.4, and 5.5.

3.2. Bayesian inference via Markov chain Monte Carlo. An important aim in time series is to learn the posterior distribution of $\boldsymbol{\theta} = (\boldsymbol{\vartheta}^\top, \boldsymbol{\beta}^\top)^\top \subseteq \boldsymbol{\Theta} \subset \mathbb{R}^{\dim_{\boldsymbol{\vartheta}} + \dim_{\boldsymbol{\beta}}}$ given realisations of the time series processes $Y_t \in \mathbb{R}$ and $\mathbf{X}_t \in \mathbb{R}^{\dim_{\mathbf{X}}}$. Let $p(\mathbf{Z}|\boldsymbol{\theta})$ denote the likelihood function of $\boldsymbol{\theta}$ given the pseudo data $\mathbf{Z} = (Z_1, \dots, Z_T)^\top$, which depends on the subset $\boldsymbol{\beta}$ of the parameter vector $\boldsymbol{\theta}$, but we suppress this dependence for notational simplicity. When the likelihood is obtained via the Whittle log-likelihood in (3.9), $p(\mathbf{Z}|\boldsymbol{\theta}) = \exp(\ell_W(\boldsymbol{\theta}))$. The likelihood function in this case is given the periodogram ordinates data $\mathbf{I} = (I(\omega_0), \dots, I(\omega_{(T-1)/2}))^\top$, but since they are functions of \mathbf{Z} we keep using the notation $p(\mathbf{Z}|\boldsymbol{\theta})$ (rather than $p(\mathbf{I}|\boldsymbol{\theta})$).

The posterior distribution of $\boldsymbol{\theta}$ is obtained using Bayes' theorem,

$$p(\boldsymbol{\theta}|\mathbf{Z}) = \frac{p(\mathbf{Z}|\boldsymbol{\theta})p(\boldsymbol{\theta})}{p(\mathbf{Z})}, \quad p(\mathbf{Z}) = \int_{\boldsymbol{\Theta}} p(\mathbf{Z}|\boldsymbol{\theta})p(\boldsymbol{\theta})d\boldsymbol{\theta}, \quad (3.10)$$

where $p(\boldsymbol{\theta})$ is the prior distribution of $\boldsymbol{\theta}$. Markov chain Monte Carlo methods are a class of iterative procedures to sample from (3.10), with the Metropolis-Hastings algorithm (Metropolis et al., 1953; Hastings, 1970) arguably being the most popular. The

Metropolis-Hastings algorithm constructs a Markov chain $\{\theta^{(j)}\}$ by starting at some initial value $\theta^{(0)}$ and then, recursively, proposes a candidate draw θ' from a proposal density $q(\theta|\theta^{(j-1)})$ and sets $\theta^{(j)} = \theta'$ with acceptance probability

$$\alpha_{\text{MH}} = \min \left(1, \frac{p(\mathbf{Z}|\theta')p(\theta')/q(\theta'|\theta^{(j-1)})}{p(\mathbf{Z}|\theta^{(j-1)})p(\theta^{(j-1)})/q(\theta^{(j-1)}|\theta')} \right). \quad (3.11)$$

If a proposed draw is rejected, $\theta^{(j)} = \theta^{(j-1)}$. The proposal density is often a random walk, e.g.

$$q(\theta|\theta^{(j-1)}) = \mathcal{N}(\theta|\theta^{(j-1)}, c\Sigma_{\text{prop}}), \quad (3.12)$$

where $\mathcal{N}(x|\mu, \Sigma)$ denotes the multivariate normal density of x with mean μ and covariance matrix Σ . Moreover, Σ_{prop} is an approximation of the posterior covariance matrix, for example minus the inverse of the observed Fisher information evaluated at the maximum a posteriori (MAP) estimate, and $c = 2.38/\sqrt{\dim(\theta)}$ for optimality, resulting in $\alpha_{\text{MH}} = 0.234$ (Gelman et al., 1997). However, in the presence of intricate geometry in the posterior due to complex dependence structures, selecting a proposal covariance as described may yield low acceptance probabilities. An alternative approach that we implement is to adaptively tune the proposal covariance matrix (Haario et al., 2001). This technique uses the information accumulated thus far through the previous draws to adjust the covariance proposal matrix. The adaptive approach can lead to more accurate simulated approximations of the target posterior and less auto-correlation in the resulting chain. To target a specified overall acceptance rate of the sampler (0.234), we follow Garthwaite et al. (2016) who utilise a Robbins-Monro search process to compute the scaling constant c in (3.12) of the adapted proposal covariance matrix.

The acceptance probability in (3.11) is set so that, informally speaking, the Markov chain consists of samples from the posterior in (3.10) after a warm-up period referred to as the burn-in. Let $\{\theta^{(j)}\}_{j=1, \dots, N}$ be the samples after discarding the burn-in. If the algorithm rejects too often, the Markov chain (the samples) becomes “sticky”, which causes inefficient estimates of posterior expectations. To explain how this inefficiency is measured, suppose θ is scalar-valued and consider estimating the expectation of a function h , i.e.

$$\mathbb{E}(h(\theta)) = \int_{\Theta} h(\theta)p(\theta|\mathbf{Z})d\theta. \quad (3.13)$$

By the weak law of large numbers,

$$\hat{\mathcal{I}}_N = \frac{1}{N} \sum_{i=1}^N h(\theta^{(i)}) \xrightarrow{P} \mathbb{E}(h(\theta)). \quad (3.14)$$

If the samples are independent, then the asymptotic variance of $\sqrt{N}\hat{\mathcal{I}}_N$ is σ_h^2 , where $\sigma_h^2 = \text{Var}(h(\theta))$. However, MCMC results in correlated samples and then the asymptotic variance of $\sqrt{N}\hat{\mathcal{I}}_N$ is $\sigma_h^2(1 + \sum_{i=1}^{\infty} \rho_i)$, where ρ_i is the autocorrelation at the i th lag of the Markov chain. The term $(1 + \sum_{i=1}^{\infty} \rho_i)$ is called the inefficiency factor. It measures how much the asymptotic variance of the estimate of a posterior expectation is inflated compared to an ideal sampler that produces independent draws. The effective sample size (ESS) of the resulting Markov chain is defined as $\text{ESS} = N / (1 + \sum_{i=1}^{\infty} \rho_i)$ (note that $\text{ESS} = N$ with independent samples). Thus, the effective sample size estimates the number of samples equivalent to the number of independent samples the sampler is generating, see Geyer (2011) for more details.

3.3. Parameterisations and prior distributions. The autoregressive parameters ϕ_i are reparameterised in terms of partial autocorrelations $-1 < \tilde{\phi}_i < 1$, for $i = 1, \dots, p$, following Barndorff-Nielsen and Schou (1973) to ensure the process is always stationary. For the moving average parameters ψ_j , for $j = 1, \dots, q$, the same reparameterisation in terms of $\tilde{\psi}_j$ ensures the process is always invertible and the moving average parametrisation is unique. To make the variance parameter σ_ε^2 and the tempering parameter λ unrestricted, we reparameterise using log-transformations. For the ARTFIMA process, the fractional parameter d ($\notin \mathbb{Z}$) is unrestricted (since stationarity does not depend on d). For ARFIMA models, on the other hand, $-0.5 < d < 0.5$ is a necessary condition for stationarity. We thus reparameterise d to an unrestricted parameter \tilde{d} by the scaled Fisher transformation $\tilde{d} = \text{arctanh}(2d)$.

When using a sample from the multivariate normal proposal as described in Section 3.2, a prior on the interval $(-1, 1)$ for each autoregressive and moving average parameter ensures $|\tilde{\phi}_i| < 1$ and $|\tilde{\psi}_j| < 1$ for the i and j above. We set independent (within and between) uniform priors $\boldsymbol{\phi} \sim \text{Unif}(-1, 1)^p$ and $\boldsymbol{\psi} \sim \text{Unif}(-1, 1)^q$. The priors for $\log(\sigma_\varepsilon^2)$ and $\log(\lambda)$ are $\mathcal{N}(0, 100)$. For the ARTFIMA process $d \sim \mathcal{N}(0, 1)$, while for ARFIMA models, the prior $\tilde{d} \sim \mathcal{N}(0, 1)$ implies a weakly informative one on $(-0.5, 0.5)$ for d . Finally, β_k , for $k = 1, \dots, m$, are assigned independent $\mathcal{N}(0, 100)$ priors. We have verified that our results are not influenced by the choice of prior (because the datasets studied are very large).

4. SIMULATION STUDIES

4.1. Accuracy of the approximation of the time domain likelihood. We compare posterior inference via the Whittle likelihood to those using the exact Gaussian and Kalman filter likelihoods under the same weakly informative priors for dynamic linear regression models on simulated data. By the exact Gaussian likelihood, we mean evaluating

a multivariate normal density where the covariance matrix is computed from the autocovariance function. The Kalman filter likelihood performs the analytic filtering steps recursively to compute the likelihood (Hamilton, 2020). Unlike the Gaussian likelihood approach, the Kalman filter avoids inverting a large covariance matrix. Note that both methods use the same (exact) time-domain likelihood, but are evaluated differently. This example is restricted to an ARMA process as the ARFIMA/ARTFIMA likelihoods cannot be efficiently evaluated using the Kalman filter (recall from Section 1 that they do not have finite-dimensional state space representations).

Let $y_t = \beta_1 x_t + \eta_t$ where η_t is an ARMA(3,1) model with $T = 5,001$. We simulate using the true value $\beta_1 = \beta_1^{(0)} = 3$ and the reparameterised vector $(\psi_1^{(0)} = \tilde{\psi}_1^{(0)})$

$$\boldsymbol{\vartheta}^{(0)} = \left(\tilde{\phi}_1^{(0)}, \tilde{\phi}_2^{(0)}, \tilde{\phi}_3^{(0)}, \psi_1^{(0)}, \log(\sigma_\varepsilon^{2(0)}) \right)^\top = (0.4, -0.2, 0.1, 0.2, \log(2))^\top,$$

and with $(\phi_1^{(0)}, \phi_2^{(0)}, \phi_3^{(0)})^\top = (0.5, -0.248, 0.1)^\top$ in the original parameterisation, where the superscript $^{(0)}$ denotes a true value. The exogenous predictor x_t is assumed to be known and is simulated from an ARMA(2,2) process. The MCMC algorithm described in Section 3.2 is used to sample the three posteriors for 10,000 iterations with a burn-in of 3,000 samples. Table 1 reports the mean squared error (MSE) of the posterior mean for 1,000 replicates of the data for each parameter. The MSE of both the Whittle likelihood and the Gaussian likelihood are small and the differences are likely attributed to Monte Carlo error.

MSE	β_1	ϕ_1	ϕ_2	ϕ_3	θ_1	σ^2
Gaussian	0.013	0.076	0.007	0.003	0.072	0.002
Whittle	0.014	0.065	0.006	0.002	0.063	0.002

TABLE 1. The mean square error (MSE) for posterior means (reparameterised) with the Gaussian likelihood and Whittle likelihood under the same prior for 1,000 data simulation replicates.

Figure 2 plots kernel density estimates of the marginal posteriors for each parameter given data from one simulation. As shown, the three posteriors are almost identical. Hence, the $n = 2,500$ periodogram ordinates were enough to get a very close approximation of the Whittle likelihood to the true time domain likelihood.

Figure 3 reports the effective sample sizes. The figure shows that the Gaussian likelihood has a $\approx 25\%$ higher ESS for the β_1 parameter compared to the Whittle likelihood and the Kalman filter likelihood. The Whittle approach has a lower ESS for σ^2 compared to its time domain counterparts. The AR and MA parameters are comparable for all three posteriors, with the Whittle posterior having slightly higher ESS for all.

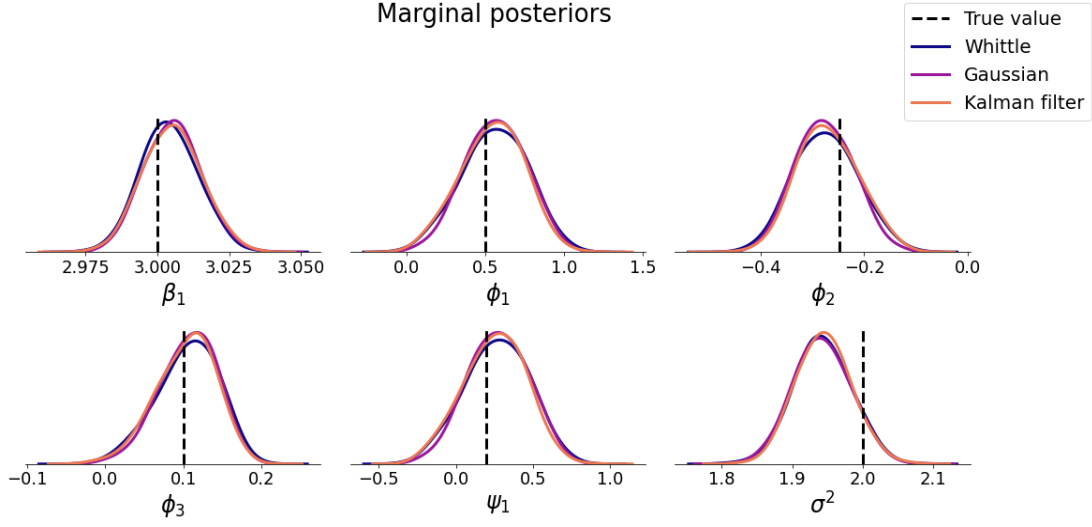


FIGURE 2. Kernel density estimates of the marginal Whittle, Kalman filter and Gaussian posteriors (original parameterisation) for a DLR model with $\eta_t \sim \text{ARMA}(3,1)$.

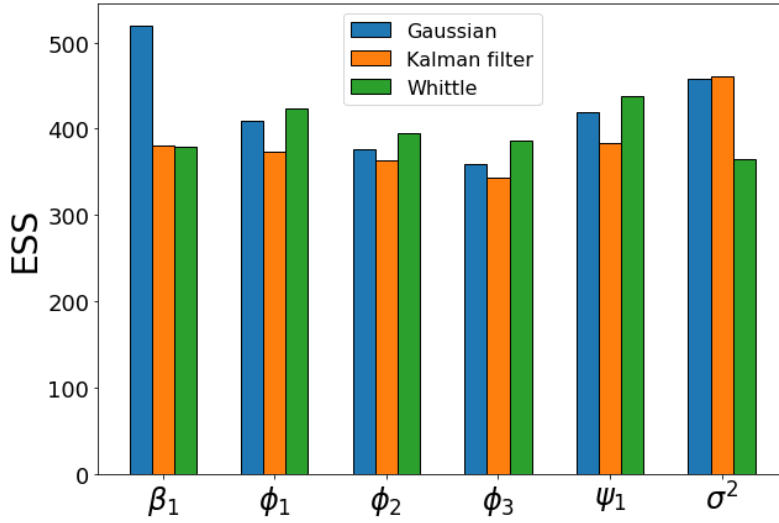


FIGURE 3. Effective sample sizes for 10,000 MCMC iterations for each parameter (original parameterisation) in a DLR model with $\eta_t \sim \text{ARMA}(3,1)$. The results are shown for the 3 methods in the legend.

Table 2 presents the run times (seconds) of each method. The proposed Whittle approach is roughly 8 times faster than the Gaussian likelihood and 94 times faster than the Kalman filter. The Gaussian likelihood uses the `SuperGauss` package in R (Ling and Lysy, 2017), which scales as $\mathcal{O}(T \log^2(T))$ using the superfast Toeplitz algorithm

proposed in Ammar and Gragg (1988). Despite the Kalman filtering being performed in $\mathcal{O}(T)$ operations, the algorithm sweeps through all observations recursively for each new MCMC proposal and is thus time-consuming, especially in the Python implementation used in this paper. The Whittle log-likelihood (3.9), on the other hand, is a simple sum that only requires computing $I_Z(\omega)$ in (3.5) and the relevant spectral density, and is thus much faster than the Kalman filter.

Run time	Whittle	Gaussian	Kalman filter
total (s)	10.0	80.54	942.58

TABLE 2. Computation time (seconds) for sampling 10,000 MCMC draws for each method.

4.2. The periodogram distribution for low frequencies. This section empirically verifies the periodogram distribution for small frequencies for the DLR with ARTFIMA errors. We also illustrate how this fails in the case of an ARFIMA error process. In a non-DLR setting, i.e. $\beta = 0$, the latter has been investigated theoretically in Robinson (1995); Rousseau et al. (2012) and empirically in Meerschaert et al. (2014); Sabzikar et al. (2019). The aim of this simulation study is to empirically verify that the ARTFIMA scaled low-frequency periodogram observations of the pseudo data in (3.5) follows (3.6), and that it is violated in the ARFIMA case.

Consider the models $y_t = \beta_1 x_t + \eta_t^{(i)}$ for $i = 1, 2$,

$$\eta^{(1)} \sim \text{ARTFIMA}(2, d, \lambda, 0), \quad \eta^{(2)} \sim \text{ARFIMA}(2, d, \lambda, 0),$$

and $x_t \sim \text{ARMA}(1, 1)$ (fixed throughout the simulation and the same for both processes). We simulate the models with $\beta_1 = \beta_1^{(0)} = 0.1$ and process parameters:

$$(i = 1) \quad \boldsymbol{\theta}^{(0)} = (\phi_1^{(0)}, \phi_2^{(0)}, d^{(0)}, \lambda^{(0)}, \sigma^{2(0)})^\top = (0.742, 0.227, 2.139, 0.616, 1)^\top,$$

$$(i = 2) \quad \boldsymbol{\theta}^{(0)} = (\phi_1^{(0)}, \phi_2^{(0)}, d^{(0)}, \sigma^{2(0)})^\top = (1.466, -0.525, 0.493, 1)^\top.$$

The parameter values of the error processes are chosen to match those obtained by the real data application in Section 5.5. Recall from (3.6) that the ratio of the periodogram and its spectrum follows the distribution

$$\frac{I_Z(\omega_k; \beta_1)}{f(\omega_k; \boldsymbol{\theta})} \sim \frac{\chi^2(2)}{2}, \quad (4.1)$$

as $T \rightarrow \infty$ for $\omega_k = \frac{2\pi k}{T}, k \in \mathcal{K}$, where \mathcal{K} is defined in (3.2) and the dependence of the parameters is emphasised. Note that if we set $\beta_1 = \beta_1^{(0)}$ when computing the periodogram, then this corresponds to the known results in a non-DLR setting since the pseudo data in (3.1) by the construction of the simulation follows an ARTFIMA (or ARFIMA) process. To obtain $\beta_1 \neq \beta_1^{(0)}$, we evaluate the periodogram at the MAP $\hat{\beta}_1$

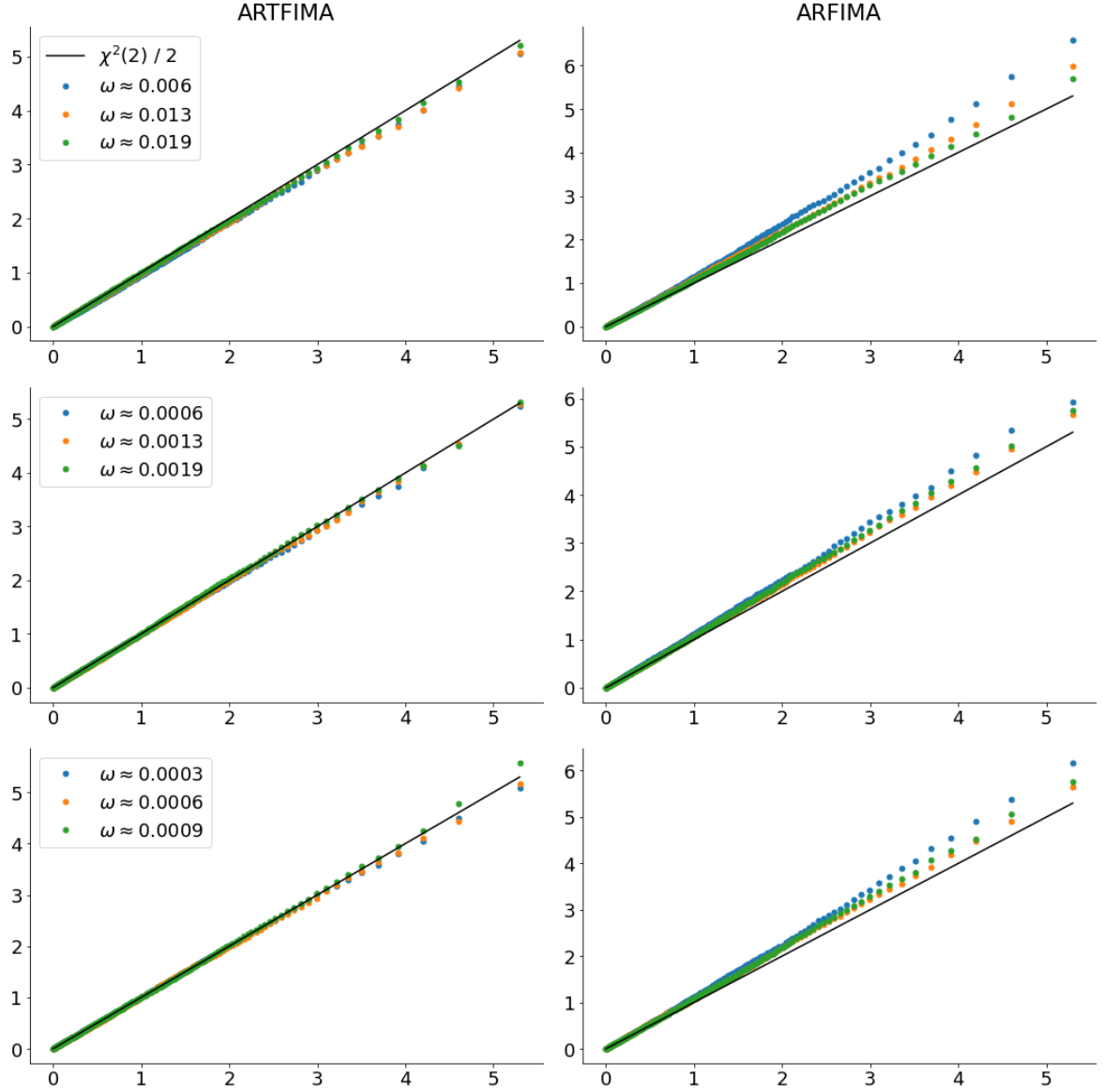


FIGURE 4. Quantile-quantile (QQ) plots of the ratio ($\hat{\beta}_1$ varying over replicates) $I_Z(\omega_k; \hat{\beta}_1) / f(\omega_k; \boldsymbol{\vartheta}^{(0)})$ for simulated DLR ARTFIMA (left panel) vs DLR ARFIMA (right panel) models for the three lowest positive frequencies. The top row, middle row, and bottom row, correspond to $T = 1,001$, $T = 10,001$, and $T = 20,001$, respectively.

in each replication. We verify (4.1) with $\boldsymbol{\vartheta} = \boldsymbol{\vartheta}^{(0)}$ and $\beta_1 = \hat{\beta}_1$ by simulating 10,000 realisations for $T = 1,001, 10,001, 20,001$ and keeping the three smallest positive Fourier frequencies ω_k (excluding zero). Figure 4 displays the quantile-quantile (QQ) plots of

$I_Z(\omega_k; \hat{\beta}_1) / f(\omega_k; \boldsymbol{\vartheta}^{(0)})$ against $\chi_2^2/2$ for all three cases of T . The left and right panels display the plots for the ARTFIMA and ARFIMA models, respectively. The upper, middle, and bottom rows correspond to $T = 1,001$, $T = 10,001$ and $T = 20,001$, respectively. The left panel (ARTFIMA) of Figure 4 shows that for the three lowest frequencies, the empirical quantiles of the periodogram ratios are almost identical to their theoretical counterpart for all T . This confirms the suitability of (4.1) for the small frequencies in the ARTFIMA model case. In contrast, the right panel (ARFIMA) shows that (4.1) is unsuitable for the small frequencies in the ARFIMA model case, and that an increasing T does not make (4.1) more suitable.

The violation of (4.1) is partly attributed to the fact that the spectrum of the ARFIMA model behaves as a power law and diverges as $\omega \rightarrow 0$. Sabzikar et al. (2019) and Meerschaert et al. (2014) show that for applications such as hydrology, finance, and climatology, the ARFIMA spectral density provides a poor fit of the periodogram at the low frequencies. We show the same issue in a dynamic linear regression model with ARFIMA errors; see Figure 9 in Section 5.4. A pragmatic solution is to use a low-frequency cutoff in the estimation of ARFIMA models in the frequency domain; however, this incurs a substantial loss of information in the estimation of the long-memory parameter d . Section 5 thus uses the exact Gaussian likelihood for dynamic linear models with ARFIMA errors, which corresponds to the exact maximum likelihood approach in Doornik and Ooms (2004). The resulting computation is much slower than a frequency domain approach and stresses the importance of our contribution, namely: a computationally fast dynamic linear model that accounts for long-range dependence in the error process.

5. APPLICATIONS

5.1. Overview and objectives. This section analyses electricity demand as the response variable conditional on relevant exogenous variables for two real-world datasets. The two datasets contain data for New England, United States of America (Example 1), and Victoria, Australia (Example 2), presented in Sections 5.4 and 5.5, respectively. Forecasting for Example 2 is considerably more challenging than for Example 1 and we show that accounting for long-range dependence is essential to obtain good forecast accuracy for moderately long horizons. In contrast, long-range dependency does not improve the forecasts in Example 1; however, we show it has a significant impact on the posterior distribution of the regression parameters β .

We compare the estimation times and forecasting abilities of models with three types of error processes: ARTFIMA, ARFIMA, and ARMA. Section 5.2 discusses the choice

of model settings and Section 5.3 presents the metrics used for the forecasting evaluation. Additionally, Example 1 illustrates the failure of a dynamic linear model with an ARFIMA error process to fit the observed power spectrum for the low frequencies.

5.2. Model settings. We consider three types of error processes: ARTFIMA, ARFIMA and ARMA. To choose the order of p and q , a search over the model space is considered up to a maximum of $p = 2, q = 1$. For various orders of p and q , we select the model with the smallest deviance information criterion (DIC) value (Spiegelhalter et al., 2002). For a given model \mathcal{M} , the deviance is defined as

$$D(\boldsymbol{\theta}) = -2 \log p(\mathbf{y}|\boldsymbol{\theta}, \mathcal{M}) + 2 \log h(\mathbf{y}), \quad (5.1)$$

where $h(\mathbf{y})$ is a fully specified standardising term which is a function of only the data, which we set to be $h(\mathbf{y}) = 1$ for all models. The DIC consists of two components,

$$DIC = \overline{D}(\boldsymbol{\theta}) + p_D, \quad (5.2)$$

where the first term is the posterior expectation of the deviance in (5.1),

$$\overline{D}(\boldsymbol{\theta}) = \mathbb{E} [D(\boldsymbol{\theta})] = \mathbb{E} [-2 \log p(\mathbf{y}|\boldsymbol{\theta}, \mathcal{M})].$$

The first term in (5.2) assesses how well the model fits the data, with smaller values being preferred. The second component, p_D , is the effective number of parameters of the model, which penalises the complexity of the model,

$$p_D = \overline{D}(\boldsymbol{\theta}) - D(\boldsymbol{\theta}^*) = \mathbb{E} [-2 \log p(\mathbf{y}|\boldsymbol{\theta}, \mathcal{M})] + 2 \log p(\mathbf{y}|\boldsymbol{\theta}^*, \mathcal{M}),$$

where $\boldsymbol{\theta}^*$ is the posterior mean. Thus, the DIC is a trade-off between the complexity and the adequacy of a model (Chan and Grant, 2016).

Once the best p and q are chosen for the ARMA error process, we compare the ARMA model to the ARTFIMA and ARFIMA models with the same p and q . Likewise, we find the best p and q for the ARTFIMA error process and compare it with the ARMA and ARFIMA models with the same p and q . However, this is not done for ARFIMA since performing MCMC over the whole model space under the Gaussian likelihood is impractical with the large datasets in the applications.

It is well known (e.g. Wheeler and Ionides, 2024) that the log-likelihood function for ARMA models may exhibit multimodality, for example when root or near root cancellation is present, and this is also true for ARTFIMA and ARFIMA. Moreover, the parameters d and λ introduce additional complexity to the geometry of the likelihood function. To avoid finding a poor local mode, we use global optimisation via Basin-hopping (Li and Scheraga, 1987) to find the MAP estimate, which serves as an initial starting value for MCMC.

5.3. Settings for forecast evaluation. For a given p and q determined as described in Section 5.2, we perform time series leave-future-out-cross-validation to evaluate the forecasting performance. We follow Hyndman and Athanasopoulos (2021, Ch. 7, Ch. 10) and assume all exogenous variables \mathbf{X}_t are known when forecasting. We use a sliding/rolling window approach with a fixed training size of T with $k = 100$ out-of-sample observations for testing. To compare models, we use three different metrics: log-predictive density score (LPDS), root mean square error (RMSE) and continuous rank probability score (CRPS). We compute each metric for different forecast horizons, $h = 1, \dots, 15$ and note that the h -step ahead case results in $k - h + 1$ out-of-sample observations ($k = 100$). Each time the window is rolled forward (to predict the next out-of-sample observation), we re-estimate the model and forecast h -steps-ahead. However, for ARFIMA, the model is only estimated once on the initial training set; this is because re-estimating the model is very costly due to the evaluation of the Gaussian likelihood. This does not have a large impact since the sliding window approach only impacts the posterior negligibly due to the large amount of data. We note that approximate leave-future-out cross-validation techniques have been proposed (Bürkner et al., 2020) for computing the LPDS that do not require reestimating the posterior. The other metrics used in this paper, however, require the posterior samples and the cost of computing the LPDS is negligible given these samples. Hence we do not implement Bürkner et al. (2020).

The h -step-ahead log-predictive density score (LPDS) is

$$\text{LPDS}^{(h)} = \frac{1}{k - h + 1} \sum_{i=0}^{k-h} \log p(y_{T+h+i} | y_{1+i:T+i}),$$

where the y_{T+h+i} for $i = 0, \dots, k - h$ are the out-of-sample observations for which we evaluate the log-predictive density,

$$\begin{aligned} \log p(y_{T+h+i} | y_{1+i:T+i}) &= \log \int_{\Theta} p(y_{T+h+i} | \boldsymbol{\theta}, y_{1+i:T+i}) p(\boldsymbol{\theta} | y_{1+i:T+i}) d\boldsymbol{\theta}, \\ &\approx \log \left(\frac{1}{M} \sum_{m=1}^M p(y_{T+h+i} | \boldsymbol{\theta}^{(m)}, y_{1+i:T+i}) \right), \end{aligned}$$

and the last line is a Monte Carlo approximation thereof, with $\boldsymbol{\theta}^{(m)} \sim p(\boldsymbol{\theta} | y_{1+i:T+i})$ and $M = 900$. The LPDS gives a measure of how well the model fits the out-of-sample data (Gelman et al., 2014), with larger values being preferred. The other two measures (RMSE and CRPS), however, have a reciprocal scale (smaller is better), and thus, we report the negative LPDS so that smaller values are preferred for all three metrics.

To assess point forecasts from a given model, define the conditional expectation when predicting the i th out-of-sample observation as

$$\hat{y}_{T+h+i} = E[\tilde{y}_{T+h+i}|y_{1+i:T+i}] = \int \tilde{y}_{T+h+i} p(\tilde{y}_{T+h+i}|y_{1+i:T+i}) d\tilde{y}_{T+h+i}, \quad i = 0, \dots, k-h,$$

where $p(\tilde{y}_{T+h+i}|y_{1+i:T+i})$ is the posterior predictive distribution. To evaluate the performance of the point forecasts, the root mean square error (RMSE) is computed as

$$\text{RMSE}^{(h)} = \sqrt{\frac{1}{k-h+1} \sum_{i=0}^{k-h} (y_{T+h+i} - \hat{y}_{T+h+i})^2},$$

for each forecast horizon h . The RMSE is the square root of the average squared distance between the out-of-sample observations and their forecasted values, and thus, smaller values are preferred.

The distributional forecasts $F()$ are assessed via the continuous rank probability score (CRPS), which is defined as

$$\text{CRPS}_i^{(h)}(F, y_{T+h+i}) = \int_{\mathbb{R}} \left(F(\tilde{y}_{T+h+i}) - \mathbf{1}\{y_{T+h+i} \leq \tilde{y}_{T+h+i}\} \right)^2 d\tilde{y}_{T+h+i},$$

where $\mathbf{1}$ is the indicator function, taking value one if $y_{T+h+i} \leq \tilde{y}_{T+h+i}$ or zero otherwise (Matheson and Winkler, 1976). When the distributional forecasts F and the data distribution are equal, the CRPS achieves its minimum and thus smaller values are preferred. The distributional forecasts are unknown but can be estimated using samples from the h -step-ahead predictive posterior distribution to estimate the empirical cumulative distribution function $\hat{F}(\hat{y}_{T+h+i})$ for all, $i = 0, \dots, k-h$. The final CRPS is formed by taking the mean over the out-of-sample observations, i.e.

$$\text{CRPS}^{(h)} = \frac{1}{k-h+1} \sum_{i=0}^{k-h} \text{CRPS}_i^{(h)}(F, y_{T+h+i}).$$

To compute the RMSE and CRPS, we use 900 samples from the posterior predictive.

5.4. Example 1: New England electricity demand. The New England data consists of hourly electricity demand (megawatts) and temperature (degrees Celsius) for the states of Maine and Vermont from 1st March 2003 to April 30th, 2017, with $T = 124,200$ observations presented in Hong et al. (2016). The response, Maine electricity demand y_t , is modelled as a linear combination of lagged exogenous variables, Maine temperature $x_{1,t-1}$ and Vermont (neighbouring state) electricity demand $x_{2,t-1}$. Strong multi-seasonal and trend components exist within each variable. The `mstl` function in the R package `Forecast` (Hyndman and Khandakar, 2008) is used to remove these effects. Figure 5 plots each variable after removing the multi-seasonal and trend components and applying a Box-Cox transformation (Box and Cox, 1964). The figure shows that the

response exhibits some long memory, making it a suitable candidate for an ARFIMA or ARTFIMA error process.

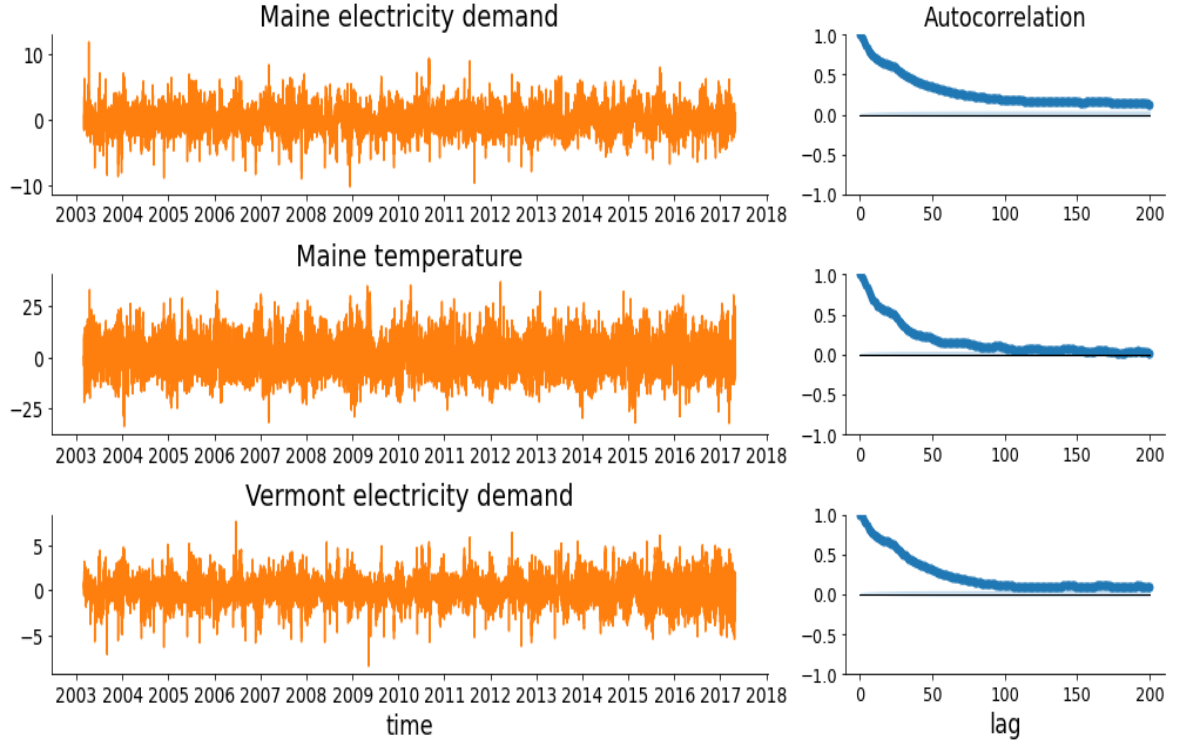


FIGURE 5. The left panels plot the Maine and Vermont hourly electricity demand and temperature data each after removing multi-seasonal and trend components and applying a Box-Cox transformation. The right panels are the corresponding autocorrelation plots.

The lowest DIC for ARMA and ARTFIMA error processes occurred for $p = 2$ and $q = 1$ in both cases. Table 3 reports the DIC values for the three models as well as the average time for one evaluation of the log-likelihood function. The table shows that ARTFIMA has the lowest DIC value, followed by ARFIMA, with ARMA having the highest (recall that lower is better). However, ARFIMA is the most computationally demanding model and is roughly 40 times slower than the other two models since the Whittle likelihood cannot be used. ARTFIMA and ARMA have comparable computational time per iteration of the log-likelihood of 11.5ms and 10.5ms, respectively.

Figure 6 plots the negative LPDS, RMSE and CRPS for each model over the forecast horizon h . For the negative LPDS, ARFIMA performs the best here for $h > 3$, and the results for ARMA and ARTFIMA are almost identical. Hence, there is no visual distinction between the two. Looking at the RMSE, the ARFIMA model has the

	ARTFIMA(2, d , λ , 1)	ARFIMA(2, d , 1)	ARMA(2, 1)
DIC	71987.56	72155.15	73030.91
Time (ms)	11.3	403.0	10.5

TABLE 3. DIC values and the average time (milliseconds) for one log-likelihood evaluation for each dynamic regression model for New England electricity demand. The lowest DIC value is in boldface.

lowest score for small h ; however, when $h > 6$, the ARMA and ARTFIMA models have a lower RMSE score compared to ARFIMA. The CRPS is similar for all models, with no model clearly outperforming the others for several forecast horizons. Figure 7 plots the predictions and prediction intervals for the three error processes when predicting the electricity demand one and six hours ahead, i.e. $h = 1, 6$. All three error processes perform accurate predictions, with the prediction intervals getting wider for larger horizons as expected. To summarise the results, we conclude that ARMA and ARTFIMA overall provide better scores and are computationally much more efficient than ARFIMA. ARMA performs almost identically to ARTFIMA, which indicates that the (semi) long-range dependency feature of ARTFIMA does not strongly influence the forecasts in this case. However, inspecting the posterior density of the regression parameter β in Figure 8 reveals a significant difference.

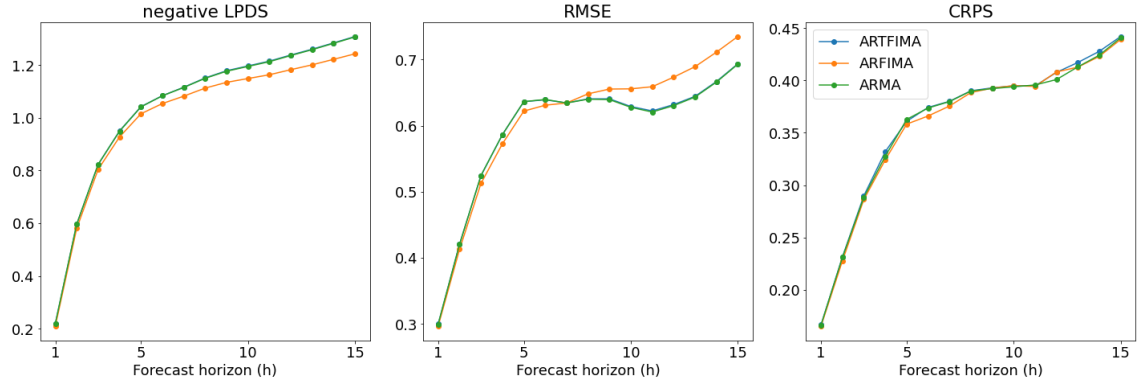


FIGURE 6. New England electricity data: negative log-predictive density score (LPDS), root mean square error (RMSE) and the continuous rank probability score (CRPS) for all models based on h -step ahead forecasts for $p = 2, q = 1$.

Finally, Figure 9 plots the fitted spectral densities (log-log scale) of the dynamic regression models with ARTFIMA and ARFIMA errors together with their corresponding periodogram data. Due to the dependence on β (estimated $\hat{\beta}$ different for the two processes), the two periodograms are different for every frequency ω but are almost identical at the lower frequencies. Consistent with the results of Sabzikar et al. (2019), the

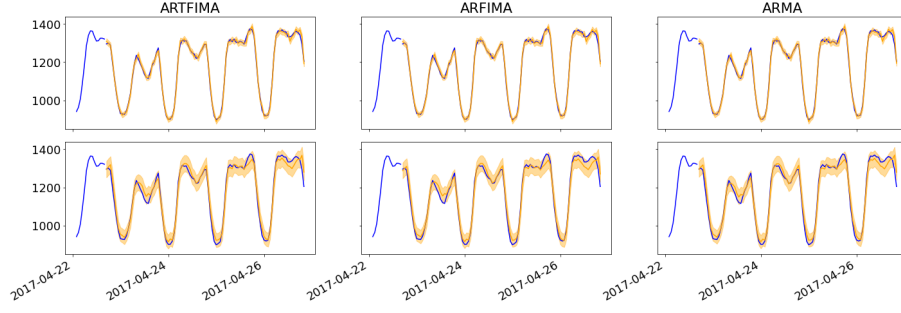


FIGURE 7. Prediction and prediction intervals for one hour ahead ($h = 1$, top panel) and ($h = 6$, bottom panel) predictions for three error processes (columns). The results are shown for New England electricity demand for $p = 2, q = 1$ after adding back the season and trend.

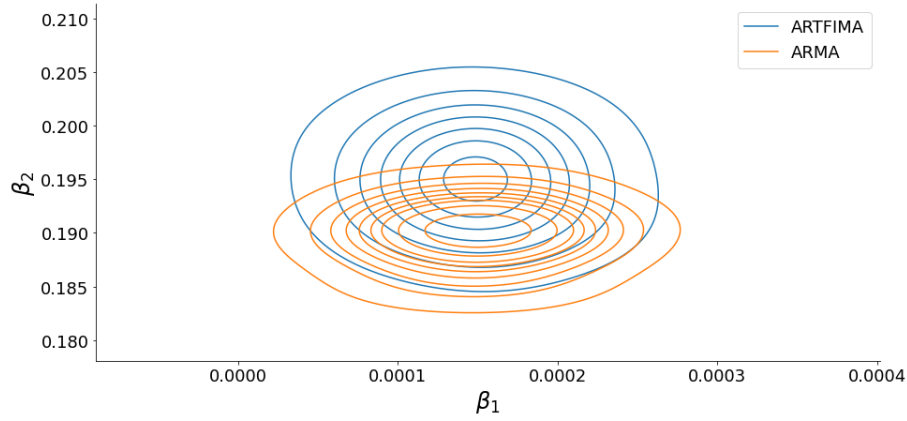


FIGURE 8. Kernel density estimates of the posterior densities of the regression parameter β using 10,000 MCMC samples. The results are for the New England data with $p = 2, q = 1$ and two error processes, ARTFIMA and ARMA.

ARTFIMA spectrum provides a better overall fit to the periodogram data, in particular for small frequencies.

5.5. Example 2: Victorian electricity demand. The second application concerns the half-hourly electricity demand for Victoria, Australia, presented in Hyndman and Athanasopoulos (2021). The data consists of $T = 52,608$ observations of electricity demand (megawatts) and Melbourne's temperature (degrees Celsius) between the 1st January 2012 - 31st December 2014. The response y_t , Victorian electricity demand, is modelled as a linear combination of the lagged exogenous variable Melbourne temperature x_{t-1} . Strong multi-seasonal and trend components exist within each variable and are

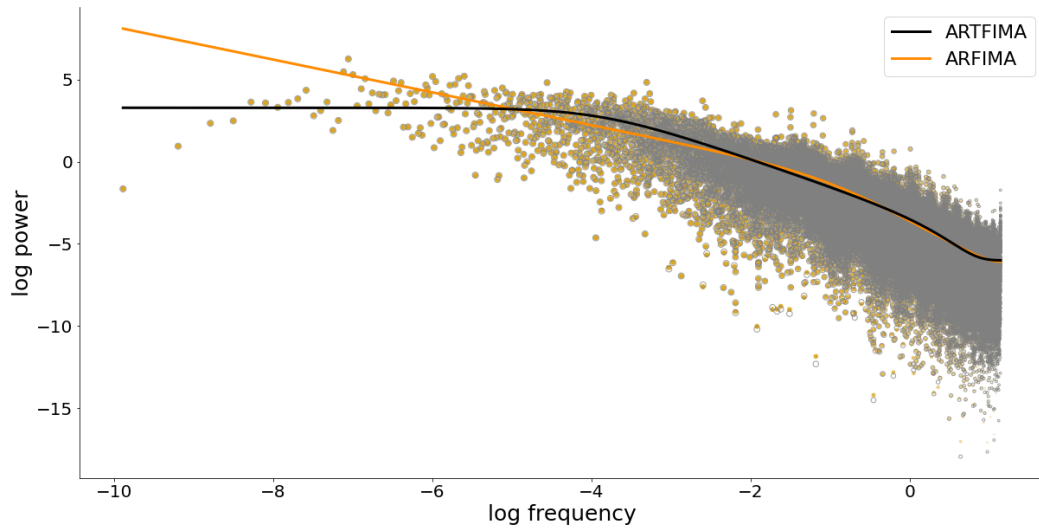


FIGURE 9. Spectral densities at the MAP and their respective periodograms. The spectrum of DLR with ARTFIMA($2, d, \lambda, 1$) errors with its periodogram (grey circles) and the DLR with ARFIMA($2, d, 1$) errors with its corresponding periodogram (orange dots).

removed via the `mstl` function. Figure 10 depicts each variable after removing the multi-seasonal and trend components and applying a Box-Cox transformation.

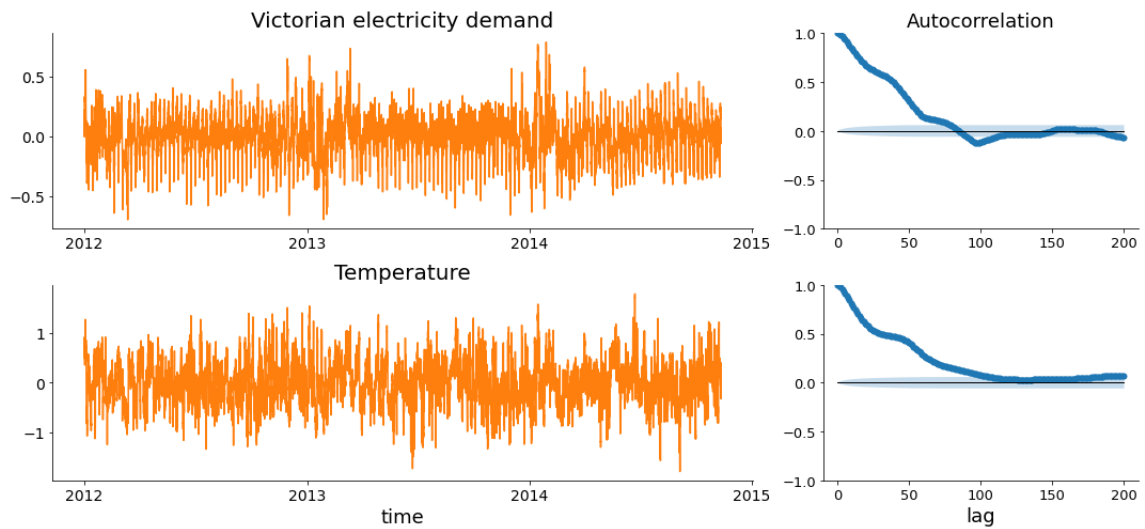


FIGURE 10. The left panels plot half-hourly electricity demand and temperature for Victoria, Australia after removing multi-seasonal and trend components and applying a Box-Cox transformation. The right panels are the corresponding autocorrelation plots.

Despite using `mstl` to remove seasonality, Figure 10 shows that all seasonality has not been removed and still exists at multiples of the 48th lag (1 day is 48 half-hours). This is also present in the periodogram, see Figure 14, which peaks at the corresponding frequencies. For this reason, we include one seasonal MA term $Q = 1$ with $s = 48$ for ARMA and ARTFIMA and denote this parameter Ψ_1^* as in (2.3). We do not include a seasonal ARFIMA model as the Gaussian likelihood is expensive to compute and our paper has overwhelming evidence that ARTFIMA captures sufficient long-range dependence while being computationally much more efficient.

The lowest DIC for the error processes occurred for two sets of lags, $p = 2, q = 0$ (ARTFIMA) and $p = 2, q = 1$ (ARMA), which we denote as ARTFIMA($2, d, \lambda, 0$) and ARMA($2, 1$). Table 4 displays the DIC value and the average time for one log-likelihood evaluation for all models. For $p = 2, q = 0$, the lowest DIC (in bold) is the SARTFIMA model, and the worst (highest) is ARMA. ARTFIMA and ARFIMA have similar values for DIC. For the $p = 2, q = 1$ case, SARTFIMA obtained the lowest DIC (in bold), followed by SARMA. Again, ARTFIMA and ARFIMA produced similar DIC values. Referring to the computation times presented in Table 4, significant computational speedups are gained for ARTFIMA and ARMA models, which had the shortest run time out of all models due to estimation via the Whittle likelihood. This is followed by the seasonal models, which are roughly 10 times slower than their non-seasonal counterparts. The slowest run times are observed for the ARFIMA model via the exact Gaussian log-likelihood, which is approximately 50 times slower than the non-seasonal ARMA and ARTFIMA models.

	SARTFIMA	ARTFIMA	ARFIMA	SARMA	ARMA
$p = 2, q = 0$	− 341016.47	−328624.02	−328612.70	−338582.68	−327041.24
$p = 2, q = 1$	− 341541.07	−328514.60	−328587.06	−338646.40	−328085.01
Time (ms)	35.1ms	3.96ms	203.0ms	35.1ms	3.79ms

TABLE 4. DIC values and the average time (milliseconds) for one log-likelihood evaluation for each dynamic regression model for Victorian electricity demand.

Figure 11 reports the forecast negative LPDS, RMSE and CRPS of the five models for the $p = 2, q = 0$ case for all horizons $h = 1, \dots, 15$. The seasonal models are better across all three metrics compared to the non-seasonal models. The seasonal ARTFIMA model has the best forecasting ability for all three metrics, closely followed by SARMA. In contrast, the ARMA model has the highest values (worst) for all three metrics. The ARTFIMA and ARFIMA models were virtually identical, having lower negative LPDS, RMSE and CRPS scores compared to ARMA.

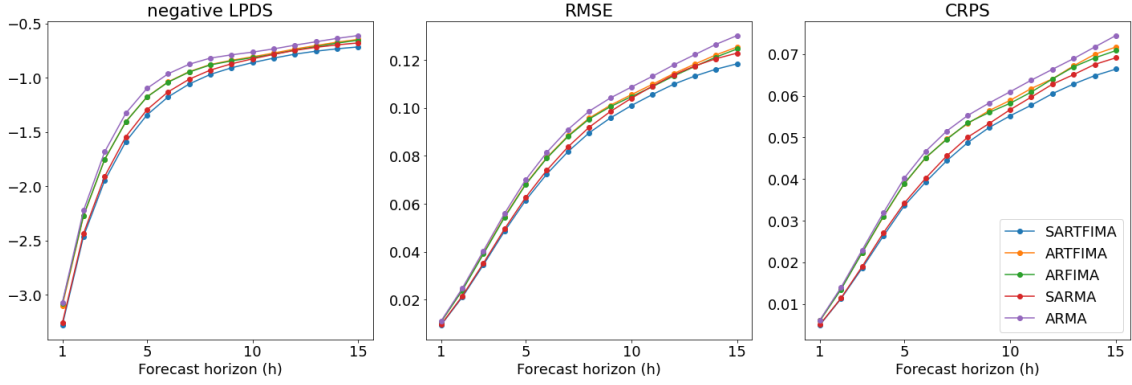


FIGURE 11. Victorian electricity data: negative log-predictive density score (LPDS), root mean square error (RMSE) and the continuous rank probability score (CRPS) for all models based on h -step ahead forecasts for $p = 2, q = 0$.

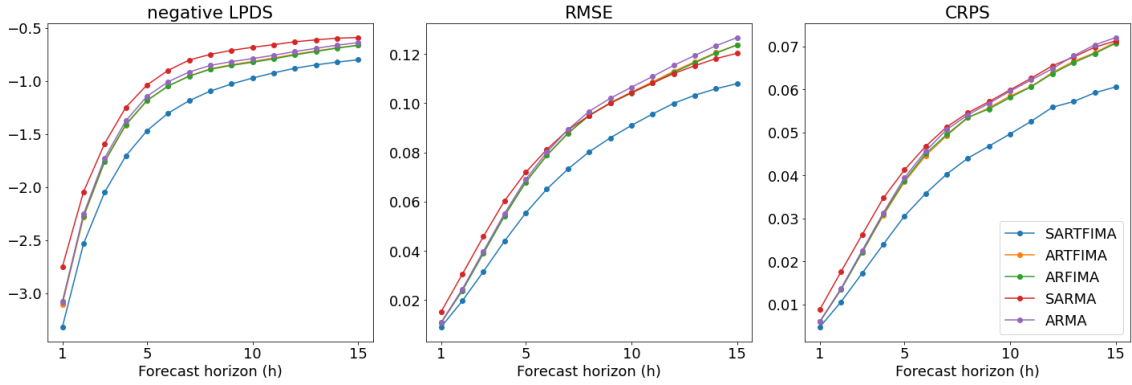


FIGURE 12. Victorian electricity data: negative log-predictive density score (LPDS), root mean square error (RMSE) and the continuous rank probability score (CRPS) for all models based on h -step ahead forecasts for $p = 2, q = 1$.

For the $p = 2, q = 1$ case, Figure 12 reports the forecast negative LPDS, RMSE and CRPS of the five models for all horizons $h = 1, \dots, 15$. The superiority of the SARTFIMA model is more pronounced compared to the $p = 2, q = 0$ case (Figure 11) across all metrics.

Figure 13 plots the predictions and prediction intervals for the seasonal models SARTFIMA and SARMA when predicting the electricity demand one and six hours ahead, i.e. $h = 2, 12$. While the one-hour ahead prediction is accurate for both models with seasonal ARTFIMA slightly more accurate, the seasonal ARTFIMA clearly performs better for the six-hours ahead forecast.

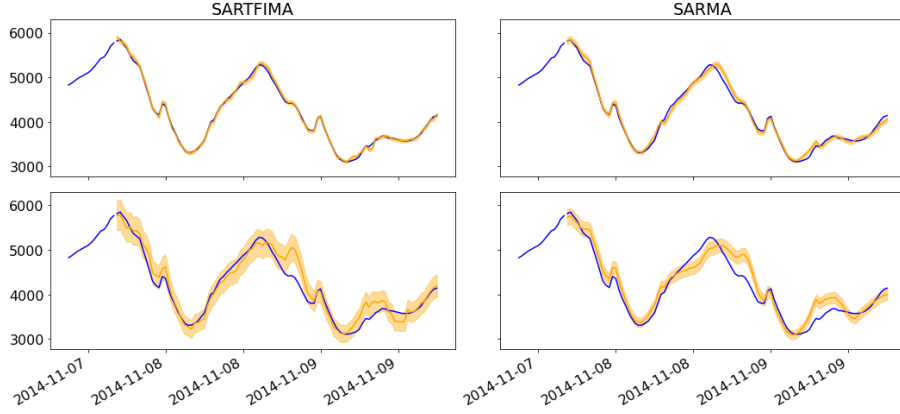


FIGURE 13. Prediction and prediction intervals for one hour ahead ($h = 2$, top panels) and six hours ahead ($h = 12$, bottom panels) predictions for the two seasonal error processes (columns) for $p = 2, q = 1$. The results are shown for Victorian electricity data after adding back the trend and seasonal components.

Finally, Figure 14 further shows the appropriateness of the seasonal ARTFIMA model by displaying a log-log plot of the periodogram and spectral density at the MAP. It is apparent that the seasonal ARTFIMA model fits the lower frequencies, $\log(\omega) < -4$, and also models the seasonal components, shown in the zoomed-in section of the plot, as it captures the peaks and troughs of the periodogram accurately.

6. CONCLUSION AND FUTURE RESEARCH

We propose a dynamic linear regression model with an ARTFIMA error process that accounts for long-range dependence. We develop a frequency domain estimation method that utilises the computationally efficient FFT. The frequency domain method uses a likelihood based on asymptotic properties of the periodogram, and we demonstrate empirically that the resulting inference matches well with time domain likelihood methods. This is expected, as the case without exogenous variables has strong theoretical results indicating that the approximation error vanishes asymptotically.

We show empirically that the well-known phenomena of the spectral density of the ARFIMA model not fitting the periodogram data well for small frequencies carries over to the dynamic linear regression case. As such, we argue that dynamic linear regression models with ARFIMA errors are unsuitable for frequency domain methods, and their estimation needs time domain methods which are computationally expensive. In contrast, we show that the dynamic linear regression models with ARTFIMA errors fit the low-frequency spectrum well and are thus a computationally fast alternative to model long-range dependence.

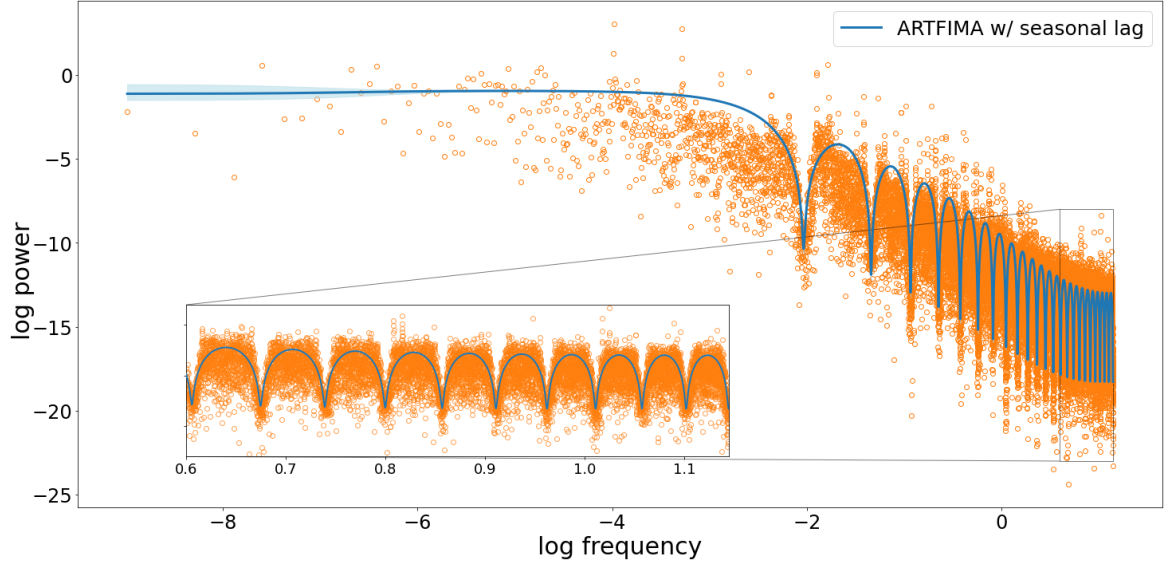


FIGURE 14. Outer plot: Log frequency vs log power (log-log) plot of the periodogram and the spectral density function at the MAP for DLR with SARTFIMA($2, d, \lambda, 1$)($0, 0, 1$)₄₈ errors. Inner plot: Same image but displaying moderate frequencies on a linear scale. The 95% credible interval of the spectral density estimated is the shaded blue region.

Our proposed models demonstrate superior forecasting performance when the data exhibits complex long-range dependence and is on par with the ARMA error process for simpler data. This is expected as our model nests the dynamic linear regression model with ARMA errors. We do not see any signs of overfitting when using an ARTFIMA error process instead of an ARMA for the simpler dataset. In addition, we also observe that the posterior distribution of the regression parameter is significantly affected by not accounting for long-range dependence in the error process. In summary, we believe dynamic linear regression models with ARTFIMA errors are robust and should be routinely included in a forecaster's toolkit.

Future research will extend our approach to modelling a multivariate response as in Villani et al. (2024). For small to moderate datasets, the Whittle log-likelihood is known to be severely biased. Exploring recent advances such as the debiased Whittle likelihood (Sykulski et al., 2019) for dynamic linear regression models can potentially enable our method to be used for small to moderately large datasets. Finally, the structure of our model can utilise subsampling MCMC methods (Quiroz et al., 2019, 2021) in the spectral domain (Salomone et al., 2020).

REFERENCES

- Ammar, G. S. and Gragg, W. B. (1988). Superfast solution of real positive definite Toeplitz systems. *SIAM Journal on Matrix Analysis and Applications*, 9(1):61–76.
- Anderson, B. D. and Moore, J. B. (2005). *Optimal Filtering*. Courier Corporation.
- Barndorff-Nielsen, O. and Schou, G. (1973). On the parametrization of autoregressive models by partial autocorrelations. *Journal of Multivariate Analysis*, 3(4):408–419.
- Bisognin, C. and Lopes, S. (2009). Properties of seasonal long memory processes. *Mathematical and Computer Modelling*, 49(9):1837–1851.
- Box, G. E. and Cox, D. R. (1964). An analysis of transformations. *Journal of the Royal Statistical Society Series B: Statistical Methodology*, 26(2):211–243.
- Box, G. E., Jenkins, G. M., Reinsel, G. C., and Ljung, G. M. (2015). *Time Series Analysis: Forecasting and Control*. John Wiley & Sons.
- Bürkner, P.-C., Gabry, J., and Vehtari, A. (2020). Approximate leave-future-out cross-validation for Bayesian time series models. *Journal of Statistical Computation and Simulation*, 90(14):2499–2523.
- Chan, J. C. and Grant, A. L. (2016). Fast computation of the deviance information criterion for latent variable models. *Computational Statistics & Data Analysis*, 100:847–859.
- Chan, N. H. and Palma, W. (1998). State space modeling of long-memory processes. *The Annals of Statistics*, 26(2):719–740.
- Cooley, J. W. and Tukey, J. W. (1965). An algorithm for the machine calculation of complex Fourier series. *Mathematics of Computation*, 19(90):297–301.
- Doornik, J. A. and Ooms, M. (2003). Computational aspects of maximum likelihood estimation of autoregressive fractionally integrated moving average models. *Computational Statistics & Data Analysis*, 42(3):333–348.
- Doornik, J. A. and Ooms, M. (2004). Inference and forecasting for ARFIMA models with an application to US and UK inflation. *Studies in Nonlinear Dynamics & Econometrics*, 8(2).
- Durbin, J. (1960). The fitting of time-series models. *Revue de l'Institut International de Statistique*, 28:233–244.
- Engle, R. F. (1974). Band spectrum regression. *International Economic Review*, 15(1):1–11.
- Garthwaite, P. H., Fan, Y., and Sisson, S. A. (2016). Adaptive optimal scaling of Metropolis-Hastings algorithms using the Robbins-Monro process. *Communications in Statistics-Theory and Methods*, 45(17):5098–5111.
- Gelman, A., Gilks, W. R., and Roberts, G. O. (1997). Weak convergence and optimal scaling of random walk Metropolis algorithms. *The Annals of Applied Probability*, 7(1):110–120.

- Gelman, A., Hwang, J., and Vehtari, A. (2014). Understanding predictive information criteria for Bayesian models. *Statistics and Computing*, 24(6):997–1016.
- Geyer, C. J. (2011). Introduction to Markov chain Monte Carlo. *Handbook of Markov Chain Monte Carlo*, 20116022(45):22.
- Granger, C. W. and Joyeux, R. (1980). An introduction to long-memory time series models and fractional differencing. *Journal of Time Series Analysis*, 1(1):15–29.
- Guyon, X. (1982). Parameter estimation for a stationary process on a d-dimensional lattice. *Biometrika*, 69(1):95–105.
- Haario, H., Saksman, E., and Tamminen, J. (2001). An adaptive Metropolis algorithm. *Bernoulli*, 7(2):223–242.
- Hamilton, J. D. (2020). *Time Series Analysis*. Princeton University Press.
- Hastings, W. (1970). Monte Carlo sampling methods using Markov Chains and their applications. *Biometrika*, 57:97–109.
- Hong, T., Pinson, P., Fan, S., Zareipour, H., Troccoli, A., and Hyndman, R. J. (2016). Probabilistic energy forecasting: Global energy forecasting competition 2014 and beyond. *International Journal of Forecasting*, 32(3):896–913.
- Hosking, J. R. (1981). Fractional differencing. *Biometrika*, 68(1):165–176.
- Hyndman, R. J. and Athanasopoulos, G. (2021). *Forecasting: Principles and Practice*. OTexts, 3rd edition.
- Hyndman, R. J. and Khandakar, Y. (2008). Automatic time series forecasting: The forecast package for R. *Journal of Statistical Software*, 27:1–22.
- Kent, J. T. and Mardia, K. V. (1996). Spectral and circulant approximations to the likelihood for stationary Gaussian random fields. *Journal of Statistical Planning and Inference*, 50(3):379–394.
- Levinson, N. (1946). The Wiener (root mean square) error criterion in filter design and prediction. *Journal of Mathematics and Physics*, 25(1-4):261–278.
- Li, Z. and Scheraga, H. A. (1987). Monte Carlo-minimization approach to the multiple-minima problem in protein folding. *Proceedings of the National Academy of Sciences*, 84(19):6611–6615.
- Ling, Y. and Lysy, M. (2017). SuperGauss: Superfast likelihood inference for stationary Gaussian time series. *R Package version*, 1.
- Matheson, J. E. and Winkler, R. L. (1976). Scoring rules for continuous probability distributions. *Management Science*, 22(10):1087–1096.
- Matsuda, Y. and Yajima, Y. (2009). Fourier analysis of irregularly spaced data on R^d . *Journal of the Royal Statistical Society: Series B (Statistical Methodology)*, 71(1):191–217.
- McLeod, A. I. and Hipel, K. W. (1978). Preservation of the rescaled adjusted range: 1. A reassessment of the Hurst phenomenon. *Water Resources Research*, 14(3):491–508.

- Meerschaert, M. M., Sabzikar, F., Phanikumar, M. S., and Zeleke, A. (2014). Tempered fractional time series model for turbulence in geophysical flows. *Journal of Statistical Mechanics: Theory and Experiment*, 2014(9):P09023.
- Metropolis, N., Rosenbluth, A. W., Rosenbluth, M. N., Teller, A. H., and Teller, E. (1953). Equation of state calculations by fast computing machines. *The Journal of Chemical Physics*, 21(6):1087–1092.
- Pankratz, A. (2012). *Forecasting with Dynamic Regression Models*. John Wiley & Sons.
- Peligrad, M. and Wu, W. B. (2010). Central limit theorem for Fourier transforms of stationary processes. *The Annals of Probability*, 38(5):2009–2022.
- Quiroz, M., Kohn, R., Villani, M., and Tran, M.-N. (2019). Speeding up MCMC by efficient data subsampling. *Journal of the American Statistical Association*, 114(526):831–843.
- Quiroz, M., Tran, M.-N., Villani, M., Kohn, R., and Dang, K.-D. (2021). The block-Poisson estimator for optimally tuned exact subsampling MCMC. *Journal of Computational and Graphical Statistics*, 30(4):877–888.
- Robinson, P. M. (1995). Log-periodogram regression of time series with long range dependence. *The Annals of Statistics*, 23(3):1048–1072.
- Rousseau, J., Chopin, N., and Liseo, B. (2012). Bayesian nonparametric estimation of the spectral density of a long or intermediate memory Gaussian process. *The Annals of Statistics*, 40(2):964 – 995.
- Sabzikar, F., McLeod, A. I., and Meerschaert, M. M. (2019). Parameter estimation for ARTFIMA time series. *Journal of Statistical Planning and Inference*, 200:129–145.
- Salomone, R., Quiroz, M., Kohn, R., Villani, M., and Tran, M.-N. (2020). Spectral subsampling MCMC for stationary time series. In *Proceedings of the 37th International Conference on Machine Learning*, volume 119, pages 8449–8458.
- Spiegelhalter, D. J., Best, N. G., Carlin, B. P., and Van Der Linde, A. (2002). Bayesian measures of model complexity and fit. *Journal of the Royal Statistical Society: Series B (Statistical Methodology)*, 64(4):583–639.
- Sykulski, A. M., Olhede, S. C., Guillaumin, A. P., Lilly, J. M., and Early, J. J. (2019). The debiased Whittle likelihood. *Biometrika*, 106(2):251–266.
- Villani, M., Quiroz, M., Kohn, R., and Salomone, R. (2024). Spectral subsampling MCMC for stationary multivariate time series with applications to vector ARTFIMA processes. *Econometrics and Statistics*, 32:98–121.
- Wheeler, J. and Ionides, E. L. (2024). Likelihood based inference for ARMA models. *arXiv preprint arXiv:2310.01198*.
- Whittle, P. (1953). Estimation and information in stationary time series. *Arkiv för matematik*, 2(5):423–434.